

Carrier dynamics and photodetection in charge injection transistors

Michael Y. Frankel

CODE 5670, Naval Research Laboratory, Washington, DC 20375-5338

Gregory L. Belenky

AT&T/Bell Laboratories, Murray Hill, New Jersey 07974 and State University of New York at Stony Brook, Stony Brook, New York 11794

Serge Luryi

State University of New York at Stony Brook, Stony Brook, New York 11794

Thomas F. Carruthers and Michael L. Dennis

CODE 5670, Naval Research Laboratory, Washington, DC 20375-5338

Alfred Y. Cho, R. A. Hamm, and Deborah L. Sivco

AT&T/Bell Laboratories, Murray Hill, New Jersey 07974

(Received 21 July 1995; accepted for publication 1 December 1995)

We study picosecond carrier transport dynamics induced by 200 fs 1.55 μm optical pulses in charge injection transistor structures. We propose and demonstrate a new optoelectronic method for exploring the interactions of hot majority carriers and cold minority carriers, as well as the optical control of real space transfer in these devices. The minority holes photogenerated in the channel produce substantial cooling of the hot-electron majority carriers and lead to the reduction of the real space transfer. The new method also provides a direct measure of the minority carrier lifetime in the transistor channel. These effects are demonstrated in InGaAs-channel devices with both InAlAs and InP barriers. The similarities in the device characteristics are explained in terms of the interaction of photogenerated minority holes with majority electrons in the channel leading to a photoconductor-like drain current and to a reduction in the real space transfer collector current. The differences are attributed to the different conduction and valence band energy offsets between the wide band gap barrier and the low band gap collector and channel layers. Furthermore, the InAlAs-barrier device shows a capability of serving as a practical photodetector with the measured, system-limited recovery speed of ~ 5 ps. © 1996 American Institute of Physics. [S0021-8979(96)08805-8]

I. INTRODUCTION

Real space transfer (RST) effects are finding increasing applications in practical semiconductor devices. For instance, charge injection transistors (CHINTs) are based on the RST of hot carriers and were originally proposed by Kastalsky and Luryi.¹ A novel transistor operating principle based on hot carrier effects makes the CHINT a useful device for studying hot majority carrier dynamics. As devices, they offer potential advantages over conventional field-effect transistors (FETs) that include: microwave performance superior to that of FETs as has been experimentally demonstrated;^{2,3} device symmetry producing output independent of input signal polarity and allowing for a direct XOR gate implementation; a single device modified to have three input terminals allowing for direct NOR and NAND gate implementation;⁴⁻⁶ light-emitting configurations are readily achievable⁷ with possible extensions to CHINT-based lasers; negative differential resistance over some operating regions makes the device useful for oscillator applications; high output nonlinearity may make CHINTs suitable for mixer applications. Thus, a gamut of properties makes CHINTs advantageous for multifunction optoelectronic integrated circuits (OEICs).⁸

The aim of the present work is twofold. First, we propose and demonstrate a new optoelectronic method for exploring the interactions of hot majority carriers and cold mi-

nority carriers. The method can be implemented with a CHINT-type device since they operate on the principle of hot majority carrier RST. The optically generated cold minority carriers directly interact with the hot majority carrier population. The effects of these interactions are reflected by picosecond transients in the device terminal currents which are directly measured. The demonstrated combined optoelectronic method is different from and complementary to the all-optical techniques that have been used to measure the energy relaxation of hot carrier plasma,^{9,10} the relaxation of hot minority carriers due to cold majority carriers,¹¹ and the relaxation of hot carrier plasma in the presence of a cold plasma background.¹²

Second, although the operation and carrier transport in CHINTs has been investigated both theoretically and experimentally with conventional dc and microwave techniques,^{13-16,3} optoelectronic techniques provide an alternate picture and an understanding of the device's optical characteristics. Such advantages have already been demonstrated with bipolar transistors.¹⁷ The present work seeks to explore the temporal characteristics of the photoinjected carrier transport on picosecond time scales and to qualitatively correlate these characteristics with device parameters. The measurements also allow us to explore optical methods for controlling the operation of CHINT-based OEIC circuits and photodetectors that would be compatible with other CHINT-

based analog, digital, and light-emitting components. The potential benefits of CHINT-based OEICs include simplified fabrication, a direct integrability leading to more efficient circuits and improved performance and functionality incorporating photodetection, amplification, and mixing within the same active device.

II. EXPERIMENTAL CONFIGURATION

We study two types of collector-up CHINT devices—one with an InP and another with an InAlAs collector barrier, which have larger conduction band and larger valence band offsets, respectively. The device structure and fabrication procedures were identical to the ones described by Belenky *et al.*^{7,3} In brief, the InP (InAlAs)-barrier device layer structure includes an InP substrate, a 300-nm-InP ($\text{In}_{0.53}\text{Ga}_{0.47}\text{As}$) undoped buffer layer, a 100 (40) nm $\text{In}_{0.53}\text{Ga}_{0.47}\text{As}$ channel *n*-type doped $5 \cdot 10^{17} \text{ cm}^{-3}$, a 150 (80) nm InP ($\text{In}_{0.52}\text{Al}_{0.48}\text{As}$) undoped barrier, a 20 (40) nm $\text{In}_{0.53}\text{Ga}_{0.47}\text{As}$ collector layer *n*-type doped $1 \cdot 10^{19}$ ($1 \cdot 10^{18}$) cm^{-3} , and a 30 (50) nm $\text{In}_{0.53}\text{Ga}_{0.47}\text{As}$ collector contact layer *n*-type doped $5 \cdot 10^{19}$ ($1 \cdot 10^{20}$) cm^{-3} . The cross-sectional band diagrams for both types of devices under a positive collector bias are shown schematically in Fig. 1.

The measurement configuration is shown schematically in Fig. 2. The device wafer was positioned on a microwave probing station for simultaneous backside optical pulse excitation and microwave transient measurements with 60 GHz probes connected to a 50 GHz Tektronix sampling scope. The quiescent drain and collector biases were supplied through bias tees, and the sampling scope input presented a 50 Ω impedance to the device under transient conditions. The laser used for device optical excitation was an Er-fiber-

based polarization-rotation configuration operating at 1.55 μm wavelength.¹⁸ Under typical operating conditions the laser produced 200 fs pulses at a 33 MHz repetition rate and 2 mW average power. Part of the laser output was split off to a 6 GHz photodetector to provide a trigger signal for the sampling scope. The overall electrical measurement system time resolution was determined to be ~ 7 ps.

III. RESULTS AND DISCUSSION

The CHINT operating principles and electrical characteristics have been discussed extensively by others⁸ and will not be reiterated here. In the following discussion we concentrate on providing a qualitative description of the physical processes taking place in CHINTs after photoexcitation; a quantitative analysis requires sophisticated numerical modeling and is beyond the scope of this article. We have considered alternative explanations for the observed photocurrents, but only the ones offered below were found to be consistent for both device types over all bias ranges and to be conforming with dc measurements. In the following discussion all positive currents are considered to be flowing *into* the device terminals.

A. InP-barrier device

The InP-barrier CHINT was studied first since its conduction band offset $\Delta E_c = 0.25 \text{ eV}$ is smaller than the valence band offset $\Delta E_v = 0.34 \text{ eV}$ ¹⁹ and the collector current is electron dominated. Considering collector metal to be a perfect reflector, the absorption coefficient of $6.8 \cdot 10^3 \text{ cm}^{-1}$ in $\text{In}_{0.53}\text{Ga}_{0.47}\text{As}$ at 1.55 μm ²⁰ and the Fresnel reflection at the substrate surface, 8.4% of the incident optical power is absorbed in the channel and 4.2% is absorbed in the collector, creating electron-hole pairs with minimal excess energy. We estimate an optically generated density of electron-hole pairs in the channel to be $\sim 5 \cdot 10^{16} \text{ cm}^{-3}$.

Figure 3(a) shows the InP CHINT dc characteristics at a constant collector bias of $V_{cs} = 1.34 \text{ V}$. These curves indicate that the device operates in a low-field regime up to a drain bias of $\sim 0.5 \text{ V}$. Increasing the drain bias further initiates the RST current flow from the channel into the collector.

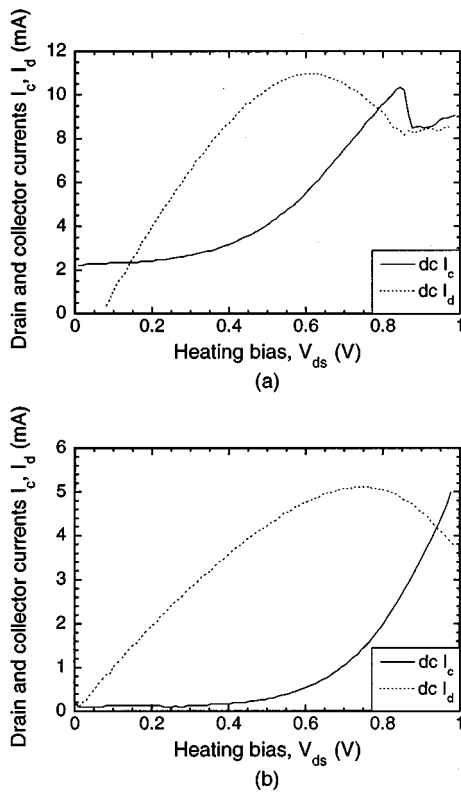


FIG. 3. Room-temperature dc characteristics of CHINTs at a constant collector bias V_{cs} : (a) InP barrier with $V_{cs}=1.34$ V, (b) InAlAs barrier with $V_{cs}=3.53$ V.

all of the transient-change currents to improve the clarity of the plots, but that actual baseline dc currents are determined by the quiescent bias conditions.

Figure 4 shows the time response of the drain current ΔI_d with the drain bias voltage V_{ds} as the parameter for the InP-barrier device. The ΔI_d response was found to be nearly independent of the collector bias, and it shows that the channel essentially functions as a photoconductor with gain. The peak ΔI_d current amplitude increases linearly with increasing V_{ds} at biases up to 0.5 V and increases superlinearly thereafter. The electrons photogenerated in the channel are rapidly swept out of the drain contact contributing to a short positive ΔI_d pulse. The channel electric field is below 5 kV/cm at V_{ds}

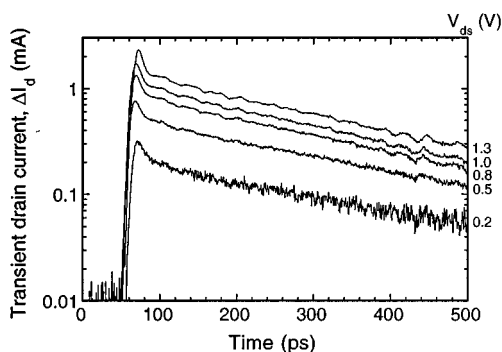


FIG. 4. Transient component of the drain currents for the InP-barrier device at $V_{cs}=0$ V with V_{ds} as parameter.

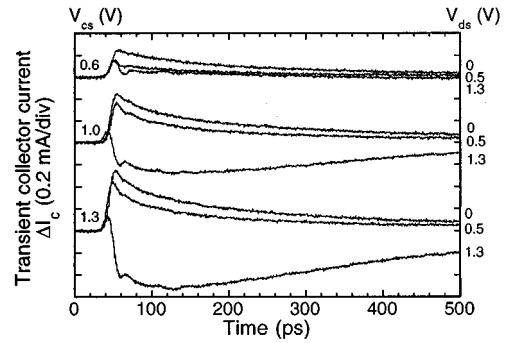


FIG. 5. Transient component of the collector currents for the InP-barrier device with V_{cs} and V_{ds} as parameters.

below 0.5 V, and the low-field hole mobility is ~ 100 $\text{cm}^2/\text{V}\cdot\text{s}$ ²¹ giving a hole sweep out time of over 200 ps. So, the relatively immobile photogenerated holes left in the channel induce additional electrons to be injected from the source and swept through to the drain contributing to the long ΔI_d tail. The tail persists until the photogenerated holes are eliminated from the channel via flow out the contact and/or recombination.

The long recovery time of ΔI_d tail stays constant at ~ 300 ps, and is completely independent of the drain bias (see Fig. 4). Since the recovery time is independent of bias, even under low-field-mobility dominated conditions, the recovery time is not determined by the hole sweep-out time. The bias independence may be explained by the large electron flux flowing from the source to the drain colliding with holes and thereby reducing the apparent hole mobility. The recovery time of the tail is then controlled by hole recombination only, which is independent of the applied bias. A definitive resolution of this question requires a detailed numerical analysis.

In contrast to the drain current ΔI_d , the collector current ΔI_c depends on both the drain and the collector biases. The bias dependence of the transient responses can be classified by three distinct regions, which also correspond to distinct dc operating regimes. Figure 5 shows current ΔI_c in three regions, (i) low V_{cs} , (ii) intermediate V_{cs} , (iii) high V_{cs} .

In the low V_{cs} region (0.6 V), there is no electron dc RST current at any V_{ds} since the effective collector barrier is increased by the applied V_{ds} near the drain where the electrons are hottest.¹⁴ At low V_{ds} , the dc collector current is dominated by electron leakage from the channel into the collector [see Fig. 3(a)], and is well described by a ~ 500 Ω resistor. The increased electron density in the channel due to photogeneration increases this component which appears as a positive ΔI_c current. The recovery time of this process is controlled by the recovery of excess carriers in the channel and is similar to the long time constant tail of the ΔI_d transients (see Fig. 4). As V_{ds} increases, the effective collector barrier increases along a larger proportion of the channel, thereby reducing the leakage current, and the transient ΔI_c current amplitude decreases. The remaining small pulse-type collector response at $V_{ds}=1.3$ V may be related to a residual displacement-type (capacitive) current component due to the large drain current transients.

In the intermediate V_{cs} region (1 V), the electron leakage from the channel into the collector is substantially increased (larger ΔI_c response) due to a reduced effective barrier all along the channel, as compared to the low V_{cs} case. Then, as V_{ds} increases, the leakage reduces (smaller ΔI_c response) due to an increasing barrier along a larger portion of the channel. As V_{ds} increases further to 1.3 V, the RST current component begins to appear in the dc characteristics. The collector current photoresponse characteristics undergo a dramatic transition, exhibited as a significant decrease in the current ΔI_c . The initial small peak in ΔI_c is again attributed to the displacement-type current as for the low V_{cs} , high V_{ds} case. In this bias region, the dc collector current is dominated by the RST of electrons from the channel into the collector. The presence of photogenerated carriers leads to a substantial decrease in this current in spite of a somewhat larger electron density in the channel. We attribute this RST-reduction effect to cooling of the hot majority electron population via inelastic collisions with cold minority holes.²² The recovery time of this component is governed by the life time of excess holes in the channel and is observed to conform to other time constants.

This explanation is consistent with the relative hot-electron scattering rate contributions due to the ionized donor impurities and cold holes.^{23,24} The scattering rates due to the two mechanisms are similar, despite an order of magnitude lower hole density. Also, the *elastic* scattering from ionized impurities leads to negligible electron energy loss, whereas the *inelastic* scattering due to holes leads directly to hot-electron cooling.

Another possible explanation for the large transient decrease in the RST current may be related to a transient decrease in the drain bias V_{ds} (and therefore reduced electron heating) caused by the increased current ΔI_d through the 50 Ω terminating resistance. This explanation is *not valid* in the regions of high V_{ds} , where the transistor characteristics are saturated and the variation in the drain bias has little effect on the current. However, a very strong transient RST current suppression is observed even under saturated conditions.

In the high V_{cs} region (1.3 V), the electron leakage component apparent at low V_{ds} is larger than that for the intermediate V_{cs} case, which again is consistent with the reduced barrier. Yet, the most substantial effect is a larger reduction of the RST current by the excess holes left in the channel, producing a substantial decrease in collector current ΔI_c at high V_{ds} . As for the intermediate V_{cs} case, the RST reduction is attributed to a cooling of the majority hot-electron population via inelastic collisions with cold minority holes. The recovery time constant is consistent with the hole lifetime in the device channel.

The above measurements provide a picture of carrier transport in CHINT transistors, with information on the magnitudes and time constants of the various picosecond transients. One of the very important conclusions to arise from these measurements is that the CHINT structure provides a good medium for investigating majority hot-electron cooling via interaction with minority cold holes. A possibility of optically controlled RST is demonstrated. The measurements also provide information on the minority carrier lifetime in

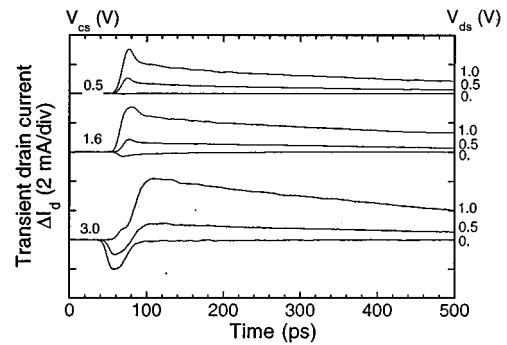


FIG. 6. Transient component of the drain currents for the InAlAs-barrier device with V_{cs} and V_{ds} as parameters.

the device channel. As for practical photodetector applications, the presence of long-lived holes decreases the device photoresponse bandwidth quite substantially. To improve the photodetection bandwidth, the holes will need to be eliminated rapidly from the device.

B. InAlAs-barrier device

One possible rapid hole elimination venue would be a CHINT with a valence band barrier offset ΔE_v much smaller than the conduction band offset ΔE_c . Conveniently, this turns out to be the case for the InAlAs-barrier devices with $\Delta E_v = 0.2$ eV and $\Delta E_c = 0.5$ eV.¹⁹ The barrier for majority carriers (electrons) is much higher in this device than in the InP-barrier one. This leads to an additional advantage of a negligible electron leakage current in the dc characteristics and to the device ability to support much higher collector biases V_{cs} . Calculating as for the InP device, 24% of the incident optical power is absorbed in the buffer and channel and 6% is absorbed in the collector. We estimate an optically generated density of electron-hole pairs in the channel to be $\sim 2 \cdot 10^{16} \text{ cm}^{-3}$.

Figure 3(b) shows the InAlAs CHINT dc characteristics at a constant collector bias of $V_{cs} = 3.53$ V. These curves indicate that the device operates in a low-field regime up to a drain bias of -0.6 V. Increasing the drain bias further initiates RST current flow from the channel into the collector.

Similar to the InP-barrier device, the InAlAs-barrier device transient characteristics depend on biases and can be classified by three regions. The operating regions are conveniently defined as

- (i) no RST (low V_{cs} , all V_{ds}),
- (ii) initial RST (intermediate V_{cs} , high V_{ds}), and
- (iii) pronounced RST (high V_{cs} , high V_{ds}).

Yet, in contrast to the InP case, not only is the collector current ΔI_c dependent on biases, but the drain current ΔI_d shows dramatically different behavior as well. It should also be noted that the RST-dominated cases correspond to much higher V_{cs} voltages than for the InP device due to a larger conduction band barrier.

In the low V_{cs} case (0.5 V) the drain current ΔI_d , shown in the top set of curves in Fig. 6, is qualitatively similar to the one observed for the InP device. It is well described by a photoconductor-like response with a rapid electron sweep

barrier. The initial total number of photogenerated holes is independent of the bias, and the increasing hole injection rate produces a response which both increases in amplitude and has a faster recovery. This interpretation is consistent with measured characteristics. At very high biases a transit-time limited response may be reached, and may permit direct measurement of hole transport across the InAlAs barrier if higher-bandwidth measurement techniques are used.²⁵

IV. CONCLUSION

In summary, we have explored carrier dynamics in novel charge-injection transistors. A new optoelectronic method for exploring the interactions of hot majority carriers and cold minority carriers has been proposed and demonstrated. In particular, the investigated device structures permitted us to observe cooling of the hot majority electron population via collisions with cold minority holes. Two types of devices were studied—one with a dominant electron photocurrent and one with a dominant hole photocurrent response. The measurements present a picture of the transistor optoelectronic properties that complements, yet is consistent with, the one obtained with more conventional dc and microwave characterizations. The measured characteristics elucidate the influence of the device structural and material properties on the electron and hole transport within the heterostructure, as well as the transient interaction of the electron and hole populations. Improvements in the measurement time resolution may allow a direct measurement of the carrier transport time across the barrier. On the practical side, such measurements demonstrate the possibility of using optical signals to control a real space transfer process, and of using the charge-injection transistors as photoreceivers in complete optoelectronic integrated circuits.

ACKNOWLEDGMENT

The support of the Office of Naval Research is gratefully appreciated.

- ¹A. Kastalsky and S. Luryi, *IEEE Electron Dev. Lett.* **4**, 334 (1983).
- ²K. Maezawa and T. Mizutani, *Jpn. J. Appl. Phys.* **30**, 1190 (1991).
- ³G. L. Belenky, P. A. Garbinsky, P. R. Smith, S. Luryi, C. A. Y., R. A. Hamm, and D. L. Sivco, *Semicond. Sci. Technol.* **9**, 1215 (1994).
- ⁴S. Luryi, P. M. Mensz, M. R. Pinto, P. A. Garbinsky, Y. Cho, Alfred, and D. L. Sivco, *Appl. Phys. Lett.* **57**, 1787 (1990).
- ⁵H. Tian, K. W. Kim, and M. A. Littlejohn, *IEEE Trans. Electron Dev.* **39**, 2189 (1992).
- ⁶M. Mastrapasqua, S. Luryi, G. L. Belenky, P. A. Garbinsky, A. Y. Cho, and D. L. Sivco, *IEEE Trans. Electron Dev.* **40**, 1371 (1993).
- ⁷G. L. Belenky, P. A. Garbinsky, S. Luryi, M. Mastrapasqua, A. Y. Cho, R. A. Hamm, T. R. Hayes, E. J. Laskowski, D. L. Sivco, and P. R. Smith, *J. Appl. Phys.* **73**, 8618 (1993).
- ⁸Z. S. Gribnikov, K. Hess, and G. A. Kosinovsky, *J. Appl. Phys.* **77**, 1337 (1995).
- ⁹H. Kurz, K. Siebert, and M. Strahnen, *Solid State Electron.* **31**, 447 (1988).
- ¹⁰T. Gong and P. M. Fauchet, in *Proceedings of the 7th International Symposium on Ultrafast Processes in Spectroscopy 1991* (IOP, Bristol, Philadelphia, 1992), pp. 317–324.
- ¹¹T. Furuta and A. Yoshii, *Appl. Phys. Lett.* **59**, 3607 (1991).
- ¹²L. H. Acioli, M. Ulman, F. Vallee, and J. G. Fujimoto, *Appl. Phys. Lett.* **63**, 666 (1993).
- ¹³S. Luryi and M. R. Pinto, *Phys. Rev. Lett.* **67**, 2351 (1991).
- ¹⁴I. C. Kizilyalli and K. Hess, *J. Appl. Phys.* **65**, 2005 (1989).
- ¹⁵T. Akeyoshi, K. Maezawa, M. Tomizawa, and T. Mizutani, *Jpn. J. Appl. Phys.* **32**, 26 (1992).
- ¹⁶M. R. Hueschen, N. Moll, and A. Fischer-Colbrie, *Appl. Phys. Lett.* **57**, 386 (1990).
- ¹⁷M. Y. Frankel, T. F. Carruthers, and C. S. Kyono, *IEEE J. Quantum Electron.* **31**, 278 (1995).
- ¹⁸K. Tamura, E. P. Ippen, H. A. Haus, and L. E. Nelson, *Opt. Lett.* **18**, 1080 (1993).
- ¹⁹M. S. Hybertsen, *Appl. Phys. Lett.* **58**, 1759 (1991).
- ²⁰D. A. Humphreys, R. J. King, D. Jenkins, and A. J. Moseley, *Electron. Lett.* **21**, 1187 (1985).
- ²¹J. R. Hayes, A. R. Adams, and P. D. Greene, *Low-Field Carrier Mobility, GaInAsP Alloy Semiconductors* (Wiley, New York, 1982), p. 204.
- ²²J. F. Young, P. Kelly, and N. L. Henry, *Phys. Rev. B* **36**, 4535 (1987).
- ²³A. F. J. Levi and Y. Yafet, *Appl. Phys. Lett.* **51**, 42 (1987).
- ²⁴A. F. J. Levi, J. R. Hayes, and R. Bhat, *Appl. Phys. Lett.* **48**, 1609 (1986).
- ²⁵M. Y. Frankel, J. F. Whitaker, and G. A. Mourou, *IEEE J. Quantum Electron.* **28**, 2313 (1992).